Observations at the tidal plume front of a high-volume river outflow

Philip M. Orton[1,2] and David A. Jay[3]

[1]   We present shipboard observations of very strong convergence, vertical velocities and mixing, and near-bed impacts associated with the leading-edge front of the tidally-pulsed Columbia River plume. With upwelling-favorable winds and riverflow of 4900 $m^3 s^{-1}$, the plume propagates as a buoyant gravity current with a rotary, bore-like vertical frontal circulation and downwelling as strong as 0.35 m s^{-1}. In waters as deep as 65 m, near-bed currents intensify to as much as 1.0 m s^{-1} after frontal passage, and are often associated with elevated acoustic backscatter. Mixing is locally strong, with an eddy diffusivity of O(0.2 $m^2 s^{-1}$) 50 m behind the front, and *T-S* diagrams imply plume mixing with 10 m deep ocean water. These observations indicate that the leading-edge front of a surface-advected plume can cause exchanges of (a) nutrients between cold subsurface shelf waters and the river plume, and (b) nutrients and sediments across the sediment-water interface. **Citation:** Orton, P. M., and D. A. Jay (2005), Observations at the tidal plume front of a high-volume river outflow, *Geophys. Res. Lett.*, *32*, L11605, doi:10.1029/2005GL022372.

1.   Introduction

[2]   Much of the interaction between river plumes and the coastal ocean occurs at the seaward boundary of each successive ebb tidal pulse [*Luketina and Imberger*, 1989], the tidal plume front. Plumes with a low Kelvin number – the ratio of river mouth width to internal deformation radius – propagate as buoyant gravity currents, with a bore-like head trailing the tidal plume front [*O'Donnell et al.*, 1998].

[3]   Observations of mixing rates in major river plumes, and especially at plume fronts, are uncommon due to the difficulty of making microstructure measurements close to the sea surface in locations with strong currents and vertical shear. This dearth of observations limits the ability of modelers to accurately simulate plume evolution [*Garvine*, 1999]. In this article, we present observations from the tidal plume front of the Columbia River plume, a high-volume plume with a mixing layer that extends to an average of 15 m depth. After describing plume front structure, propagation rate, velocity and near-bed acoustic backscatter, we analyze mixing using *T-S* diagrams and a Thorpe overturn length-scale analysis. To conclude, we discuss the broader implications of these observations with respect

to coastal ocean nutrients and ecosystems. Observed ecological impacts are discussed elsewhere [*Morgan et al.*, 2005].

2.   Measurements and Analyses

[4]   From 24–27 May 2001, two vessels and a helicopter mapped the Columbia's daily greater-ebb tidal plume front as it propagated out to sea. Each day, winds were from the N or NW at 5–10 m s^{-1}, and ambient ocean currents from the N at 0.10–0.20 m s^{-1}. River flow varied from 4500–5100 $m^3 s^{-1}$ (relative to a summer mean of ~5000 $m^3 s^{-1}$), and daily tidal range from 2.46–2.55 m (a moderate spring tide). These winds, ocean currents, tides and river flows are typical of the summertime upwelling-dominated regime and plume conditions. Also, the pattern and velocity of front propagation during ebb tide was similar each day. Because forcing variability was small enough that plume and front characteristics were similar on each day, data from all four days are pooled in this paper and viewed with respect to tidal phase (hours past higher-high water, HHW).

[5]   To observe frontal conditions, we towed a horizontally mounted Ocean Sensors Model OS200 CTD in a "tow-yo" saw tooth pattern, with a mean horizontal speed through water of 0.91 m and descent rate of 0.63 m s^{-1}. The sampling rate was 6.3 Hz, resulting in mean horizontal and vertical resolutions of 0.14 and 0.10 m, respectively. The OS200 has a rapid-response integral conductivity-temperature sensor, and is specifically designed for fine-scale sampling. At 1 m s^{-1} speed through water, the characteristic length scale for temperature and conductivity is ~2 cm (K. McCoy, Ocean Sensors, personal communication, 2005). A 300 kHz Acoustic Doppler Current Profiler (ADCP), mounted in a well in the vessel hull, continuously measured current velocity and acoustic backscatter. Acoustic data are averages of 80 samples (35 seconds), resulting in a mean horizontal resolution of 60 m, and obscuring some fine-scale variability near the front-line. Acoustic backscatter data has been corrected for absorption and spreading.

[6]   Highly visible frontlines coincided with a maximum horizontal density gradient and strong downwelling, as observed in other studies [e.g., *O'Donnell et al.*, 1998]. For hydrographic and ADCP transect plots, we define a frontal coordinate system that is rotated so that the positive *x* direction is seaward and perpendicular to the frontline. Velocities are rotated into the frontal coordinate frame, but with absolute (not front-relative) magnitudes (u, v). We estimate the local front velocity and direction from repeated measurements of front location from two vessels and a helicopter, then verify that these estimates are reasonable using synthetic aperture radar (SAR) images for similar ocean, tide and wind conditions. Banded regions of elevated SAR backscatter are generally found in association with

[1]Lamont-Doherty Earth Observatory of Columbia University, Palisades, New York, USA.
[2]Formerly at Oregon Health and Science University, Beaverton, Oregon, USA.
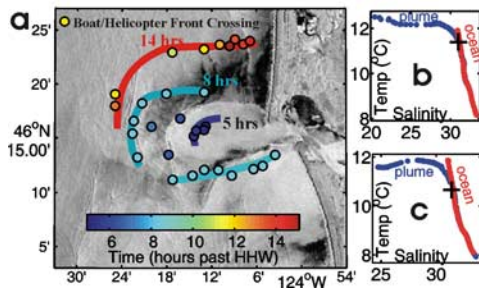[3]Oregon Health and Science University, Beaverton, Oregon, USA.

Figure 1. (a) Front-tracking map showing the progression of the front in hours after higher-high water on May 27, 2001. The grayscale background is backscatter from a satellite-borne RADARSAT-1 synthetic aperture radar (SAR) at 6.5 h, when sharp backscatter gradients clearly delineate the outer plume front. This SAR image is from a different day with similar conditions (Oct 1, 2001; Image processed at the Alaska Satellite Facility, © Canadian Space Agency). Also shown are T-S diagrams from (b) 8.5 h along the northern frontal edge (c) 6 h along the northwestern frontal edge. The base of the mixing layer is marked with a plus in *T-S* space.

strongly convergent river plume fronts (Figure 1a), due to modulation of sea surface roughness caused by the convergence at the leading edge of the front and divergence after its passage [*Hessner et al.*, 2001].

[7] To quantify plume mixing, we first define two plume layers, then describe methods for observing turbulent mixing parameters. The base of the overflow layer ($z = h_0$) is the depth above which front-normal water velocities are greater than the front itself [*Luketina and Imberger*, 1989], and we define the base of the mixing layer ($z = h_1$) as the depth where the plume profile *T-S* curve converges to the *T-S* curve from the nearest oceanic profile (within 0.1°C and 0.1 salinity; Figures 1b and 1c, '+'). To estimate the Thorpe scale L_T [*Galbraith and Kelley*, 1996], we sort each CTD density profile so that it increases monotonically and then compute mixing parameters, an approach that gives comparable results to microstructure instrumentation [e.g., *Klymak and Gregg*, 2004]. We compute L_T as the rms vertical displacement of water parcels in each overturn patch, a vertically continuous unstable region. We use strict quality control methods for avoiding spurious overturns

from measurement noise [*Galbraith and Kelley*, 1996] or from the horizontal movement of the towed platform [*Ott et al.*, 2004] (data are omitted if the ratio of sensor horizontal to vertical speed through water exceeded 10:3). Dissipation of turbulent kinetic energy is estimated as $\varepsilon = a^2 L_T^2 N^3$ and eddy diffusivity as $K_\rho = a^2 \Gamma N L_T^2$. Here, $a \approx 1$, the buoyancy frequency $N = [(g/\rho)(\partial \rho / \partial z)]^{0.5}$ is averaged through overturn patches, and the mixing efficiency $\Gamma \approx 0.22$ for coastal stratified flows [*Peters*, 1999; *Kay and Jay*, 2003; *MacDonald and Geyer*, 2004]]. Minimum detectable mixing levels for these methods may be computed from sampling parameters, mean $\partial \rho / \partial z$ during the study period, and manufacturer specified uncertainty in CTD measurements [*Galbraith and Kelley*, 1996]. For $0 < z < h_1$, the minimum detectable values within an overturn for ε and K_ρ are 4×10^{-5} W kg^{-1}, and 5×10^{-3} m²s^{-1}, respectively.

3. Results

[8] The propagation pattern of the outer edge plume front is demonstrated in Figure 1a, with in situ front-crossing locations overlain on an SAR image from a period with similar conditions. Hereafter, we focus only on measurements between 5 and 9 h past higher-high water. The time-progression of front crossing locations indicates that the mean frontal progression velocity is 0.8 m s^{-1} for the western edge and 0.6 m s^{-1} for the northern edge. Despite rapid spreading and mixing, the plume is strongly stratified, with $\partial S / \partial z$ from 2–4 m^{-1} in the upper few meters of the water column. The mean depth of the overflow layer (h_0) from 50 to 400 m behind the front is 4.8 m. The base of the mixing layer (h_1) generally shoals as time passes, and averages about 15 m. The northern frontal edge consistently had the strongest cross-front density difference during our study. This is likely a result of the southward ambient ocean currents, which consistently brought relatively high-salinity shelf waters in contact with the plume.

3.1. Strong Convergence, Downwelling and Near-Bed Impacts

[9] A transect across the northern frontal edge at 8.5 h (front velocity is 0.60 m s^{-1}) shows strong surface convergence, downwelling and reverse flow near the bed (Figure 2a). The largest velocities were typically aligned
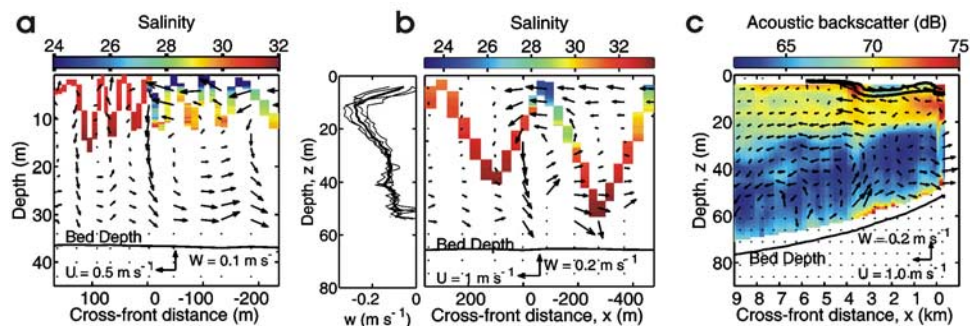

Figure 2. Observations from three transects, with vectors showing vertical and across-frontal velocity (w, u). (a) The northern frontal edge at 8.5 h. (b) The northwestern frontal edge at 6 h. The profiles of vertical velocity (w) were measured with the vessel maintaining position in the frontline for three minutes. The four thin lines are 35 s average profiles, while the thick line is a 140 s grand average. (c) A longer transect from 9 km offshore to the northwestern frontal edge at 7 h, with contours of S = 27 and 28.
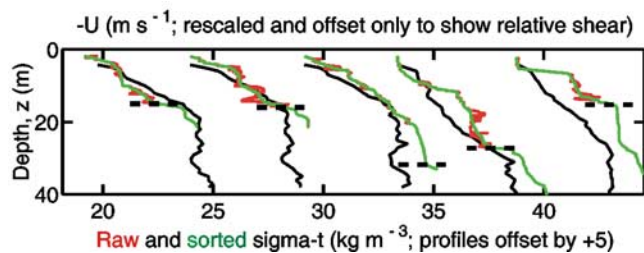
Figure 3. Five plume profiles from 5–6.5 h of raw density anomaly (raw σ_t: red) with sorted density anomaly overlaid (sorted σ_t; green), negative across-front velocity ($-u$; black), and the depth of the mixing layer (h_1; dashed line). Unstable regions, overturns, are visible where the red line is not concealed by the green line. The maximum full-profile (between 4 and 40 m) velocity difference shown is 1.4 m s^{-1}.

with the direction of front propagation, forward (near-surface) or reverse (near-bed), with only a small lateral (along-front) velocity component. Observed salinity patterns show that relatively fresh water is subducted below the front line. Full water-column S profiles (not pictured) indicate that a substantial cross-front gradient extends at least to 30 m, and possibly to the bed. Thus, frontal passage influences most or all of the water column. However, the plume profile water below ~20 m (h_1) occupies the same T-S space as ocean profile water (Figure 1b), suggesting that subsurface ocean waters are subducted below the plume with little direct mixing.

[10] A transect across the northwest plume front at 6 h shows clear vertical circulation around a gravity current head, intensified near-bed current speeds and intense downwelling of 0.35 m s^{-1} (Figure 2b). These patterns are especially strong for transects from 5–6.5 h along the northwestern frontal edge, where we observe the highest mean frontal propagation velocity (0.80 m s^{-1}), and deepest mean mixing layer depth (h_1 = 22 m). The T-S diagram (Figure 1c) shows the most obvious case in our study where plume water is mixing with subsurface ocean water, because the plume T-S curve hits the ocean curve at a T-S combination that corresponds to a shelf water parcel from 10 m depth, 10.8 °C, and 31.5 salinity. Mixing of properties (e.g., nutrients) between these two water masses can be inferred.

[11] Near-bed velocity and acoustic backscatter increase dramatically in association with front passage, with positive gradients toward the bed. Figure 2c shows a transect from offshore to the northwest plume front at 7 h (front velocity is 0.67 m s^{-1}). ADCP observations and limited CTD data show a primary front line (x = 0 km; ΔS = 9) preceded by a secondary frontline (x = 3.5 km; ΔS = 3.4) that appears to be associated with an internal wave. SAR images from 5–9 h often show alternating bands of high and low backscatter preceding the tidal plume front. In some cases, there are as many as 10 undulation cycles. Similar SAR backscatter patterns have been identified to be internal waves using theory and in situ data at other locations [*Hessner et al.*, 2001]. J. D. Nash and J. N. Moum (River plumes as a source of large amplitude internal waves in the ocean, submitted to *Nature*, 2005) present detailed observations

of internal waves or solitons generated at Columbia plume fronts.

3.2. Intense Mixing

[12] Mixing parameters are presented below as averages over $5 < t < 9$ h, $-400 < x < -50$ m and $0 < z < h_1$, then as a function of distance behind the front. Vertical averaging is employed in both cases for two reasons: (1) the plume is continuously stratified during ebb tide, with no slab-like discontinuous interface (Figure 3); (2) estimates of mixing from Thorpe scales should be averaged over many overturns. For this region and period, there are 62 CTD profiles with 233 overturn patches. The resulting averages were: L_T = 0.74 m (0.50–0.96 95% bootstrapped confidence interval), $\varepsilon = 2.4 \times 10^{-4}$ W kg^{-1} (1.0–4.0 $\times 10^{-4}$), and $K_\rho = 2.0 \times 10^{-2}$ m^2 s^{-1} (0.7–3.7 $\times 10^{-2}$). Mixing decreases after the end of ebb tide, and by 12 h, few overturns are detected in our CTD measurements.

[13] Overturns typically occurred in regions with strong density and velocity gradients (Figure 3), consistent with mixing induced by shear instability. The local gradient Richardson number is $Ri = N^2 V_z^{-2}$, where V_z is the vertical shear. Regions with high diffusivity generally coincide with subcritical Richardson number values ($Ri < 0.25$), as expected. The relationship between Ri and K_ρ for all profiles combined has substantial scatter, but generally Ri is inversely proportional to K_ρ. Of all bins with $K_\rho >$ 0.1 m^{2}s^{-1}, ~70% have $Ri < 0.25$. Of all bins with $K_\rho <$ 0.001 m^{2}s^{-1}, ~70% have $Ri > 0.25$. Vertically averaged ε and K_ρ decrease rapidly with distance behind the front (Figure 4). Maximum values of ε and K_ρ tend toward ~10^{-3} W kg^{-1} and ~0.2 m^{2}s^{-1} at 50 m behind the frontline.

4. Discussion

[14] *Luketina and Imberger* [1989] found that mixing was strong at the plume leading edge, but their maximum ε was two orders of magnitude below the mean in our study.
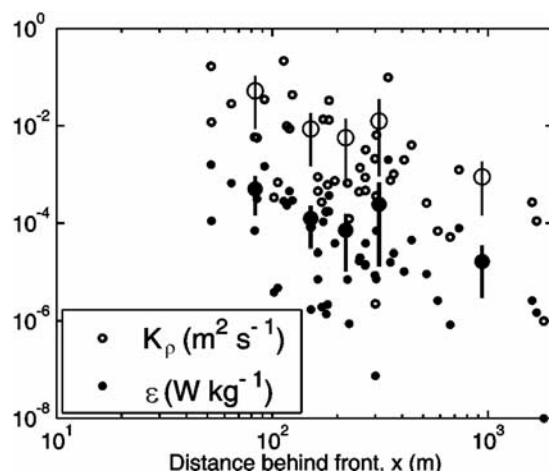

Figure 4. Mean values of dissipation (ε) and diffusivity (K_ρ) for $0 < z < h_1$ and $5 < t < 9$ h past HHW, plotted against the mean distance behind the frontline for each CTD profile. The superimposed large circles are means of each successive set of nine points, with bootstrapped 95% confidence bars.

Our maximum ε estimates are comparable to those observed at the most turbulent sites in the ocean, such as the estuarine plume lift-off zone of the Fraser River ($\varepsilon \sim 10^{-3}$ W kg^{-1}) [*MacDonald and Geyer*, 2004] or the Knight Inlet sill ($\varepsilon \sim 10^{-4}$ W kg^{-1}) [*Klymak and Gregg*, 2004]. The downwelling velocities of up to 0.35 m s^{-1} are about twice the maxima observed in other plume front studies, e.g., 0.20 m s^{-1} on the Connecticut River plume [*O'Donnell et al.*, 1998]. No previous study has estimated plume frontal K_ρ using density fine-structure.

[15] The observed inverse relationship between mixing and distance from the front (Figure 4) is consistent with prior studies that have shown that plume mixing is strongest near the tidal plume front [*Luketina and Imberger*, 1989]. Computing the vertical salt flux, $J_s = -10^{-3}\rho K_\rho \partial S/\partial z$ (in kg m^{-2}s^{-1}) [*Peters*, 1999], we estimate the plume salinization rate $J(x) = 10(-x)^{-1.6}$ using a nonlinear least-squares regression for all J_s data from $-400 < x < -50$ m, $0 < z < h_1$, and $5-9$ h. Integrating this equation over $-100 < x < -10$ m, and multiplying by the approximate mean front length (30 km), the vertical salt transport rate (with bootstrapped 95% confidence interval) is 1.1 ($\pm$0.5) $\times 10^5$ kg s^{-1}. The typical tidal outflow from the estuary and initial plume salinity (after liftoff) are 29,600 m^{3}s^{-1} and $S_0 = 15$, respectively, for the riverflow and tidal range observed in our study [*Jay et al.*, 2005]. Our observed salt transport rate is 20% of the total required to salinize these plume waters from $S_0 = 15$ to $S = 33.5$, indicating that the region within 100 m of the tidal plume front is responsible for a substantial part of total plume mixing. It is noteworthy that this region is only 2% of the plume area at 7 h.

[16] Most of the world's major river plumes, including the Columbia, are "surface-advected plumes", in that they detach from the bed before they propagate out to sea [*Yankovsky and Chapman*, 1997]. However, our observations provide a good example of how tidally-pulsed river plumes differ from the idealized steady-state plume considered by Yankovsky and Chapman: The tidal plume front and associated internal waves can cause near-bed current intensification, and therefore, surface-advected plumes can have a strong influence on the bottom boundary layer.

[17] Our results show that tidal plume fronts can cause ecologically important exchanges of (a) nutrients between cold subsurface shelf waters and the river plume, and (b) nutrients and sediments across the sediment-water interface. The observation that 10 m deep continental shelf water is directly mixing with plume water is important because nutrient signatures in the plume and coastal ocean differ significantly. Moreover, nutrient-rich upwelling water is often present at this depth during the summertime upwelling season [*Chase et al.*, 2002]. Also, recent studies suggest that resuspended bottom sediment may be an important source of iron for primary production in coastal waters worldwide, as well as the California Current that absorbs the Columbia River plume in summertime [e.g., *Chase et al.*, 2002]. We observe near-bed velocity intensification (as high as $\sim$1 m s^{-1}) below the propagating front, in even our deepest ADCP measurements of 65 m. Given low Ri values ($\sim$10^{-2}), a velocity of 1 m s^{-1} may cause a shear velocity of 5 cm s^{-1} (applying a quadratic drag law

with a drag coefficient of 0.002) [*Orton and Kineke*, 2001]. This is strong enough to erode and hold in suspension particles of up to 350 μm diameter [*Dyer*, 1986, p. 165], coarser than most continental shelf sediments, and cause a flux of bioavailable iron into the water column.

[18] In conclusion, our observations of intense localized mixing behind the tidal plume front of a surface-advected river plume confirm that these fronts play a major role in the vertical transfer of buoyancy and other constituents. Future studies of river plumes should also monitor the bottom boundary layer, because the deepwater impacts we have observed may also cause ecologically relevant exchanges of constituents across the sediment-water interface.

References

Chase, Z., A. van Geen, P. M. Kosro, J. Marra, and P. A. Wheeler (2002), Iron, nutrient, and phytoplankton distributions in Oregon coastal waters, *J. Geophys. Res.*, *107*(C10), 3174, doi:10.1029/2001JC000987.

Dyer, K. R. (1986), *Coastal and Estuarine Sediment Dynamics*, 342 pp., Wiley-Interscience, Hoboken, N. J.

Galbraith, P. S., and D. E. Kelley (1996), Identifying overturns in CTD profiles, *J. Atmos. Oceanic Technol.*, *13*, 688–702.

Garvine, R. W. (1999), Penetration of a buoyant coastal discharge onto the continental shelf: A numerical model experiment, *J. Phys. Oceanogr.*, *29*, 1892–1909.

Hessner, K., A. Rubino, P. Brandt, and W. Alpers (2001), The Rhine outflow plume studied by the analysis of synthetic aperture radar data and numerical simulations, *J. Phys. Oceanogr.*, *31*, 3030–3044.

Jay, D. A., C. N. Cudaback, and T. A. Chisholm (2005), Impacts of maintenance dredging at the mouth of the Columbia River on plume salinity, project report, 153 pp, U.S. Army Corps of Eng., Portland, Oreg., in press.

Kay, D. J., and D. A. Jay (2003), Interfacial mixing in a highly stratified estuary: 1. Characteristics of mixing, *J. Geophys. Res.*, *108*(C3), 3072, doi:10.1029/2000JC000252.

Klymak, J. M., and M. C. Gregg (2004), Tidally generated turbulence over the Knight Inlet sill, *J. Phys. Oceanogr.*, *34*, 1135–1151.

Luketina, D. A., and J. Imberger (1989), Turbulence and entrainment in a buoyant surface plume, *J. Geophys. Res.*, *94*, 12,619–12,636.

MacDonald, D. G., and W. R. Geyer (2004), Turbulent energy production and entrainment at a highly stratified estuarine front, *J. Geophys. Res.*, *109*, C05004, doi:10.1029/2003JC002094.

Morgan, C. A., A. de Robertis, and R. W. Zabel (2005), Columbia River plume fronts: Hydrography, I., zooplankton distribution, and community composition, *Mar. Ecol. Prog. Ser.*, in press.

O'Donnell, J., G. O. Marmorino, and C. L. Trump (1998), Convergence and downwelling at a river plume front, *J. Phys. Oceanogr.*, *28*, 1481–1495.

Orton, P. M., and G. C. Kineke (2001), Comparing calculated and observed vertical suspended sediment distributions from a Hudson River Estuary turbidity maximum, *Estuarine Coastal Shelf Sci.*, *52*, 401–410.

Ott, M. W., J. A. Barth, and A. Y. Erofeev (2004), Microstructure measurements from a towed undulating platform, *J. Atmos. Oceanic Technol.*, *21*, 1621–1632.

Peters, H. (1999), Spatial and temporal variability of turbulent mixing in an estuary, *J. Mar. Res.*, *57*, 805–845.

Yankovsky, A. E., and D. C. Chapman (1997), A simple theory for the fate of buoyant coastal discharges, *J. Phys. Oceanogr.*, *27*, 1386–1401.

D. A. Jay, Oregon Health and Science University, 20000 NW Walker Rd., Beaverton, OR 97006, USA.

P. M. Orton, Lamont-Doherty Earth Observatory of Columbia University, 61 Route 9W, Palisades, NY 10964, USA. (orton@ldeo.columbia.edu)